Electrostatic calibration method for large-amplitude dynamic Casimir force measurements

Song Cui*
*Institute of Materials Research and Engineering (IMRE), Agency for Science, Technology and Research (A*STAR), 3 Research Link, 117602 Singapore*

Yeng Chai Soh†
School of Electrical and Electronic Engineering, Nanyang Technological University, 50 Nanyang Avenue, 639798 Singapore
(Received 21 July 2012; published 9 October 2012)

Electrostatic calibration is important in Casimir force measurements. It is necessary for the estimation of the unknown system parameters such as the absolute separation distance and the identification of the electrostatic force model. Correct estimates of the unknown parameters and the electrostatic force model are crucial for interpreting the Casimir force data. In this paper, we present an electrostatic calibration method with higher sensitivity and robustness. It is based on large-amplitude dynamic force measurements. It is proven in theory that the unknown system parameters can be obtained accurately and the electrostatic force model can be identified by our method. The effectiveness and robustness of our method are tested on synthetic data with added noise when the Casimir force measurement is conducted between a sphere and a flat surface.

DOI: 10.1103/PhysRevA.86.042504 PACS number(s): 31.30.jh, 06.20.−f, 84.37.+q

I. INTRODUCTION

The Casimir force exists between two electrically neutral and nonmagnetic bodies [1]. The Casimir effect is a macroscopic phenomenon of quantum mechanics, which can be explained by zero-point electromagnetic energy. There is significant interest in studying the origin of the Casimir force and how it is modified by temperature, material properties, and geometries of the interacting materials [2–4]. It is interesting to explore the relationship between the Casimir force and the four fundamental forces, which may help generalize unification theories [5]. The understanding of the Casimir force also contributes to the progress of elementary-particle, atomic, and condensed-matter physics [6]. Besides, the Casimir force is an important design factor in nanoeletromechanical systems [7].

In order to verify various hypotheses and theories of the Casimir force, extensive experiments were performed during the last decade at the submicrometer level based on atomic force microscopy (AFM) [8] and micromachined torsional balance [9]. The first precise measurement was conducted in a vacuum environment between a sphere and a flat plate, both coated with gold [10]. The issue of parallel alignment [11] was successfully avoided by using the sphere-plate configuration. Subsequently, experiments were performed between sample surfaces with a cylinder geometry [12] and complex geometries, such as sinusoidal corrugations [13] and regular trenches [14]. It was also found that the Casimir force can be altered if interacting materials are with different dielectric permittivities [15]. Recently, thermal Casimir force measurements were conducted [16,17]. In most situations, the Casimir force between interacting materials is attractive, but it can be repulsive if suitable materials and mediums are chosen [18–20]. The experimental verification of the repulsive Casimir force was observed between gold and silica in the fluid bromobenzene [21], while theories predict that the repulsive Casimir force can also be observed between some novel materials in air or vacuum [22,23].

Although extensive measurements were conducted, novel instrumentation methods and data analysis techniques with better accuracy and robustness are needed [24]. Measurement uncertainties will raise the ambiguity in interpreting the experimental data [25]. Currently, there are some obstacles for improving the accuracy of the Casimir force measurements. First of all, it is a challenge to obtain an accurate estimate of the separation gap between the interacting materials in Casimir force measurements [26]. It is not easy to employ external devices to measure this quantity, as the size of the interacting materials is much larger than the separation gap in Casimir force measurements [27]. On the other hand, there are many issues and debates in modeling, characterizing, and reducing the electrostatic forces [28,29]. As electrostatic forces of different origins coexist with the Casimir force in all Casimir force experiments, any errors in characterizing electrostatic forces will directly affect the Casimir force data [30]. The conventional electrostatic calibration method [27] for calculating the separation distance and characterizing the electrostatic forces has several shortcomings. First, electrostatic calibrations are conducted at very large separations (several micrometers) in order to minimize the effect of the Casimir force. Even a 1% measurement error in R (the radius of the sphere) will lead to >10 nm of measurement errors in the separation distance estimate. This will create huge discrepancies in interpreting the Casimir force data, as some Casimir force measurements were conducted at separations below 100 nm. Second, electrostatic calibrations are conducted statically. As measurements are conducted at different separations in steps that are time consuming, the measurement accuracy will be affected by noise and drift.

In this paper, we propose an electrostatic calibration method based on large-amplitude dynamic force measurements at separations between 500 nm and 2 μm, where the electrostatic force is strong and the Casimir force cannot be neglected. This is motivated by the fact that large-amplitude dynamic force measurements are proven to be more robust and sensitive than static force measurements in the AFM community [31].

*cuis@imre.a-star.edu.sg
†eycsoh@ntu.edu.sg

Compared to small-amplitude dynamic atomic force measurements [32], the electrostatic calibration by large-amplitude force measurements can be performed without moving the piezo transducer in steps. Large-amplitude dynamic Casimir force measurements were reported in Ref. [33] and showed a significant improvement in measurement sensitivities. However, nonlinear phenomena have been predicted and observed [33–35], which leads to difficulties in interpreting the measurement results. In our previous work, we have proposed a method to estimate the absolute separation distance based on large-amplitude dynamic force measurements [36]. But this method is based on an assumption that the electrostatic force has the model of $F_e = -\pi\varepsilon_0 R[V_m^2 + V_1^2]/d$, where ε_0 is the permittivity of free space, R is the sphere radius, V_m is the contact potential difference between two interacting materials which can be neutralized, d is the separation gap, and V_1 is due to the electrostatic patch charge which is assumed to be known in that paper. In practice, it is not possible to calculate V_1 because the distribution of electrostatic patch charge is unknown and there are huge debates on different electrostatic force models [37]. All of these issues will be addressed by the proposed method in this paper. It will be shown that one is able to estimate the unknown parameters accurately via the proposed method. Its effectiveness and robustness are tested on synthetic data with noise when the Casimir force measurement is conducted between a sphere and a flat surface. At the same time, the electrostatic force model can be justified as well.

II. MODEL

Our method is based on a modified AFM where the probeless cantilever is electrically isolated and the spherical surface is mounted on the motorized actuator [29]. The measurement setup is shown in Fig. 1. Our method can also be modified for other Casimir force experimental setups like the micromachined torsional balance reported in Refs. [9,17]. A sinusoidal excitation signal is used to excite the cantilever to produce large-amplitude vibrations (hundreds of nanometers). The deflection of the cantilever is measured from the optical detector. The dynamic equation of the cantilever is given by

$$\ddot{x}(t) + 2\gamma\dot{x}(t) + \frac{k}{m}x(t) = \frac{I}{m}\sin\omega t - \frac{1}{m}\{V_1^2 F_e(n,[z+x(t)]) + F_c(z+x(t))\}, \quad (1)$$

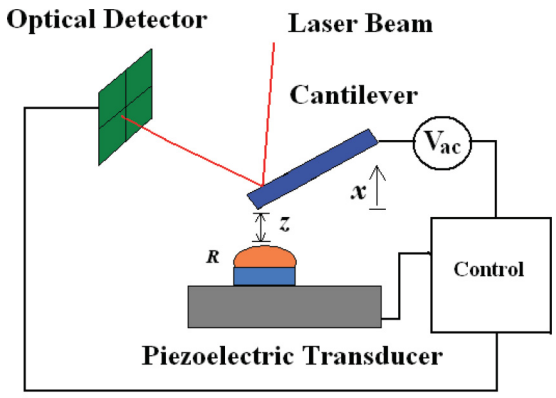

FIG. 1. (Color online) The schematic of the measurement setup.

where $x(t)$ is the instantaneous position of the cantilever end which can be measured by the deflecting optical beam, m is the effective mass of the cantilever, γ describes the system damping, k is the spring constant of the cantilever, I is the amplitude of the excitation signal, ω is the excitation frequency, $F_e(n,[z+x(t)])$ is the electrostatic force, $F_c(z+x(t))$ denotes the Casimir force between the sphere and the cantilever, and z is the separation gap when the cantilever is in equilibrium. Here we assume that the electrostatic force is partially neutralized by applying an external bias voltage and V_1 denotes the voltage difference which may be due to the electrostatic patch potential fluctuation. The residue of the electrostatic force can be modeled or approximated as the following equation:

$$F_e(n,d) = \frac{\pi\varepsilon_0 R}{d^n}, \quad (2)$$

where n is a positive number. In the literature, there were reported measurements showing that the electrostatic force model [Eq. (2)] is different from the standard model of the electrostatic force between a large sphere and a flat surface [29]. This observation suggests that the assumption of $n = 1$ without any verification is not always true, and the value of n needs to be determined. The model of the Casimir force depends on temperature, materials, and geometries. As the electrostatic calibration is conducted at a separation distance below 2 μm, the thermal effect is small compared to the electrostatic force and it is neglected here. Both the cantilever and the sphere are coated with gold. Then the Casimir force can be calculated as

$$F_c(d) = \frac{\pi^3\hbar c R}{360 d^3} r_c(d), \quad (3)$$

where $r_c(d)$ is the conductivity correction to the ideal Casimir force [38]. Here we use the approximation form of $r_c(d) = \exp(-4\delta_0/d)$ [39], where $\delta_0 = 137/2\pi$ nm is the effective penetration depth of gold. This approximation has less than 0.6% error when the separation distance is larger than 500 nm. The error can be further reduced by using higher-order approximations, but it is good enough to use this first-order approximation. As the electrostatic calibration is conducted at separations larger than 500 nm, the correction to the Casimir force due to the surface roughness is less than 0.1%, even if the roughness amplitude is 10 nm for a flat surface [40]. Thus, the roughness correction is not considered in this paper. But we point out that our method is still effective if the roughness correction or even geometry correction is considered. The objective of the electrostatic calibration is to estimate the unknown quantities z, V_1, and n based on the available measurement data of the excitation signal and the cantilever vibrations $x(t)$.

III. METHOD

Four linear filters are required in our estimation process:

$$\ddot{\xi}_1(t) + 2\gamma_1\dot{\xi}_1(t) + \frac{k}{m}\xi_1(t) = \frac{F_e(\hat{n},\hat{z}+x(t))}{m}, \quad (4)$$

$$\ddot{\xi}_2(t) + 2\gamma_1\dot{\xi}_2(t) + \frac{k}{m}\xi_2(t) = \frac{F_c(\hat{z}+x(t))}{m}, \quad (5)$$

$$\ddot{\zeta}(t) + 2\gamma_1\dot{\zeta}(t) + \frac{k}{m}\zeta(t) = \ddot{x}(t) + 2\gamma\dot{x}(t) + \frac{k}{m}x(t), \quad (6)$$

$$\ddot{\psi}(t) + 2\gamma_1\dot{\psi}(t) + \frac{k}{m}\psi(t) = \frac{I}{m}\sin\omega t, \quad (7)$$

where $\hat{n}$ is the estimate of n. Based on reported measurements, $n < 2$. Thus, the range of $\hat{n}$ can be limited to $0 < \hat{n} < 2$. Our method is still effective even if we further extend the range of $\hat{n}$ as long as Eq. (12) is satisfied. $\hat{z}$ is the estimate of z. In Eqs. (4) and (5), the force inputs to the second-order system are the estimated electrostatic force and Casimir force where the unknown separation gap z is replaced by the estimate $\hat{z}$. Other correction factors such as surface roughness can be considered in the Casimir force model as well, and our method is still effective if the unknown separation distance z is replaced by its estimate $\hat{z}$ in the proposed linear filters [Eqs. (4) and (5)]. Since collision between the sphere and the cantilever should be avoided in the real experiment, $\hat{z}$ must satisfy $[\hat{z} + x(t)] > 0$. γ_1 is chosen to satisfy $\gamma_1 > \sqrt{k/m}$. We denote that $y(t) = \psi(t) - \zeta(t)$. Although only $x(t)$ is measurable, we can get $\zeta(t)$ by passing $x(t)$ through the linear transfer function: $(s^2 + 2\gamma_1 s + k/m)/(s^2 + 2\gamma s + k/m)$. Inspired by Schwarz inequality, we construct a cost function with respect to $\hat{z}$ in the time interval $[t_1,t_2]$:

$$G(\hat{z}) = \int_{t_1}^{t_2}[y(t) - \xi_2(t)]^2 dt - \frac{\left(\int_{t_1}^{t_2}\{[y(t) - \xi_2(t)]\xi_1(t)\}dt\right)^2}{\int_{t_1}^{t_2}\left[\xi_1^2(t)\right]dt}. \quad (8)$$

When $\hat{n} = n$, it is proven in the Appendix that the cost function has the following properties under normal operation conditions:

$$\frac{dG(\hat{z})}{d\hat{z}} < 0\,(\hat{z} < z), \quad (9)$$

$$\frac{dG(\hat{z})}{d\hat{z}} = 0\,(\hat{z} = z), \quad (10)$$

$$\frac{dG(\hat{z})}{d\hat{z}} > 0\,(\hat{z} > z), \quad (11)$$

if the positive functions $F_c(x)$ and $F_e(n,x)$ with $x > 0$ satisfy the following conditions:

$$\frac{d\frac{dF_e(n,x)/dx}{F_e(n,x)}}{dx} > 0, \quad \frac{d\frac{dF_c(x)/dx}{F_e(n,x)}}{dx} > 0,$$
$$\frac{d\frac{dF_c(x)/dx}{F_c(x)}}{dx} > 0, \quad \frac{d\frac{F_c(x)}{F_e(n,x)}}{dx} < 0, \quad \frac{dF_c(x)}{dx} < 0. \quad (12)$$

It is easy to show that our electrostatic force model $F_e(n,x)$ and the Casimir force model $F_c(x)$ satisfy these conditions. In other words, the cost function $G(\hat{z})$ has only one local minimum and it will reach it only when $\hat{z} = z$. It is also proven that $G(\hat{z} = z) = 0$ [?]. Thus, optimization methods such as the gradient method and golden section search method [41] can be applied to locate the local minimum of the cost function $G(\hat{z})$. Once the accurate estimate of z is obtained, it is easy to show that V_1 can be estimated accurately:

$$\hat{V}_1 = \sqrt{\int_{t_1}^{t_2}\{[y(t) - \xi_2(t)]\xi_1(t)\}dt \Big/ \int_{t_1}^{t_2}\left[\xi_1^2(t)\right]^2 dt}. \quad (13)$$

However, if the electrostatic force model in the experiment is different from the model assumed in our estimation algorithm ($\hat{n} \neq n$), then the location of the local minimum of $G(\hat{z})$ will shift to another position where $\hat{z} \neq z$. Thus, an estimation error in absolute separation distance will be produced if the electrostatic force model assumed in our method is not correct. This is the reason why the identification of the electrostatic force model, in other words, estimating n, is important in the electrostatic calibration process.

Here, we propose to excite the cantilever vibrations at three separation distances (z_1,z_2,z_3) in order to estimate n accurately. Although it is not possible to measure directly the separation distances, it is feasible to measure their differences (e.g., $z_1 - z_2$, $z_2 - z_3$) by measuring the distances of piezo movements. The estimation processes will be conducted with different estimates of n at each separation distance. If $\hat{n} = n$ is assumed in the algorithm, then the differences in the estimated separation distances $(\hat{z}_1 - \hat{z}_2, \hat{z}_2 - \hat{z}_3)$ should be matched with measured distances of piezo movements ($z_1 - z_2$ and $z_2 - z_3$), respectively. On the other hand, if $\hat{n} \neq n$ is assumed in the algorithm, then the location of the local minimum of $G(\hat{z})$ will shift to another position where $\hat{z} \neq z$, as mentioned in the previous paragraph. As the dynamic system and $G(\hat{z})$ are highly nonlinear in nature, the amount of shift will be different if the cantilever vibrates at different separation distances. In that case, $\hat{z}_1 - \hat{z}_2$ and $\hat{z}_2 - \hat{z}_3$ will not be consistent with measured distances of piezo movements if a wrong estimate of n is assumed in our algorithm. Thus, by comparing $\hat{z}_1 - \hat{z}_2$ and $\hat{z}_2 - \hat{z}_3$ computed at different $\hat{n}$ with the piezo movement distances, we are able to estimate n accurately and identify the correct electrostatic force model. Besides the Casimir force research, accurate identification of the electrostatic force model can help us understand various electrostatic effects. As discussed above, the absolute separation distance z and V_1 can be calculated correctly once n is estimated accurately.

IV. SIMULATION STUDIES

Our method will be tested based on synthetic data generated by computer simulations. The fourth-order Runge-Kutta numerical method with a step size of 1×10^{-7} is used to simulate

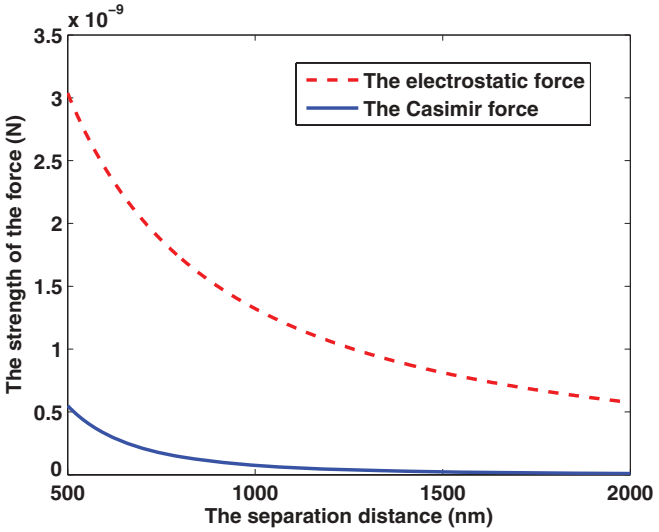

FIG. 2. (Color online) The strength of the Casimir force and the residue electrostatic force in the numerical studies.

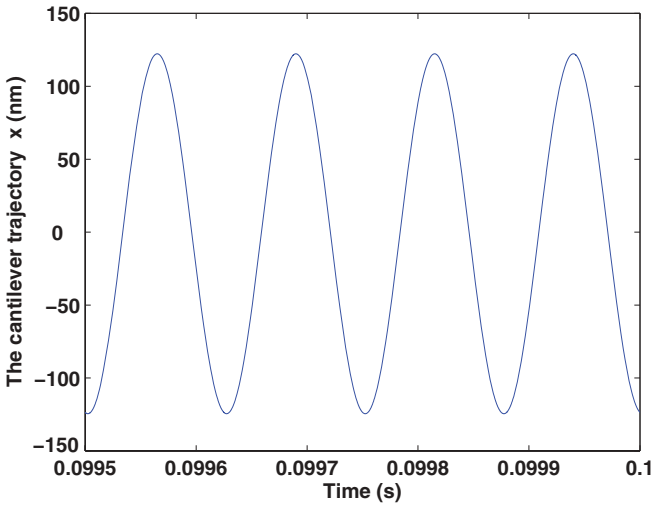

FIG. 3. (Color online) The trajectory of cantilever vibration.

the system dynamics described by Eq. (1). The system parameters used in Eq. (1) are similar to the real experiment setup reported in Ref. [29]. In all of our simulations, $R = 30$ mm, $k = 1$ N/m, $\omega_0 = \sqrt{k/m} = 2\pi \times 8$ kHz, and $\lambda = 240$ s^{-1}. The cantilever is much softer in our simulations compared to Kim's setup [29] in order to have large-amplitude vibrations. The excitation signal is set as $I/m = 3\,m/s^2$ and $\omega = \omega_0$. The electrostatic force is modeled as $F_e(d) = \frac{\pi\epsilon_0 R}{d^n}$ with $n = 1.2$. The voltage difference due to the electrostatic patch charge is chosen to be $V_1 = 10$ mV, which is in the range of theoretical predictions and experimental findings [17,42,43]. Data in the time interval [0.09,0.1] are processed in the algorithm.

Thus, the strength of the Casimir force and the electrostatic force in our numerical studies can be calculated (Fig. 2). It can be seen that the residue electrostatic force is stronger than the Casimir force when the separation distance is above 500 nm. Neglecting the Casimir force in any calibration methods in this regime will give errors in determining the absolute separation distance and characterizing the electrostatic force. Next, estimation results will be presented separately when measurement data are clean and when measurement data are subject to noise.

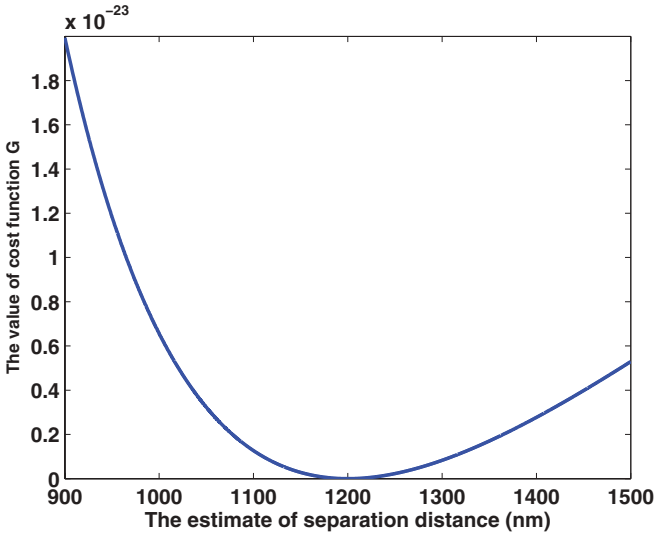

FIG. 4. (Color online) The cost function $G(\hat{z})$ with respect to $\hat{z}$.

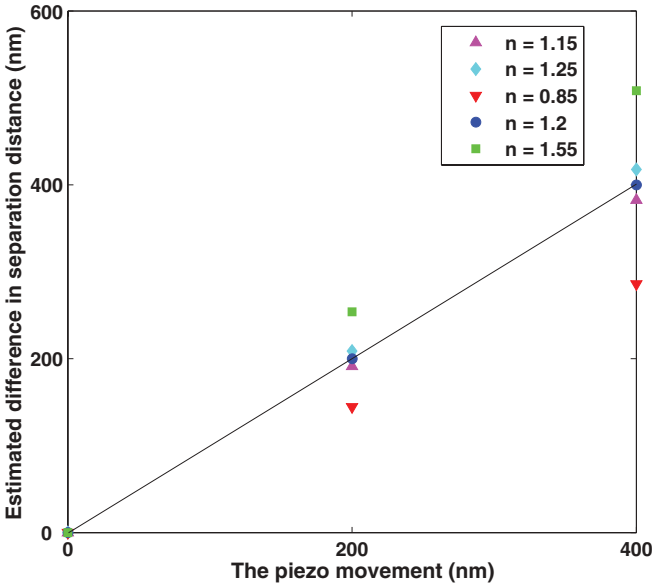

FIG. 5. (Color online) The estimated piezo movement with respect to different $\hat{n}$ when the separation distance is changed from 800 nm to 1200 nm and the measurement is free of noise.

A. Noise-free measurement data

Here, we present the estimation results produced by our method when the cantilever trajectory $x(t)$ measurement is free of noise. The cantilever-sample separation distance at the equilibrium is set to be $z = 1200$ nm. The trajectory of the cantilever vibration is plotted in Fig. 3. It can be seen that the cantilever is experiencing large-amplitude sinusoidal vibration. The cost function $G(\hat{z})$ with respect to different estimates of z is calculated when $\hat{n} = n = 1.2$. It is shown that there is only one local minimum in $G(\hat{z})$ and it is located at $\hat{z} = z = 1200$ nm (Fig. 4). Thus, if the assumption on the electrostatic force model is correct, then it is able to find the

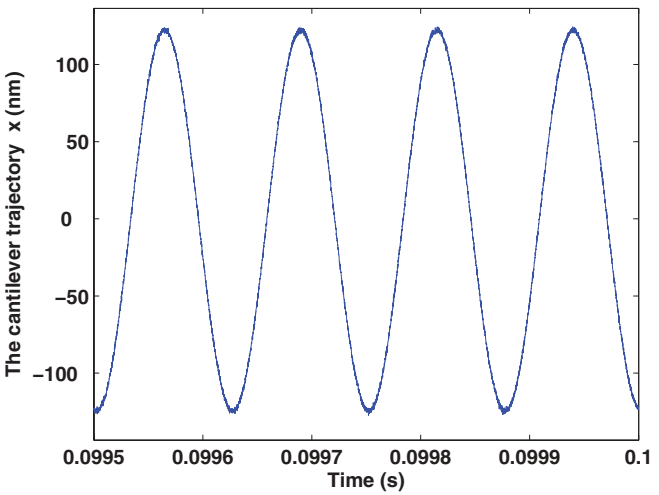

FIG. 6. (Color online) The trajectory of cantilever vibration with Gaussian noise.

TABLE I. Estimated separation distance (nm) when the measurement is noiseless.

z (nm)	$\hat{n} = 0.9$	$\hat{n} = 1$	$\hat{n} = 1.1$	$\hat{n} = 1.2$	$\hat{n} = 1.3$	$\hat{n} = 1.4$	$\hat{n} = 1.5$
800	688.07	721.93	759.38	800.00	843.65	890.29	939.08
1000	839.55	888.51	942.16	1000.00	1061.57	1126.14	1193.01
1200	988.90	1053.91	1124.51	1200.00	1279.38	1362.05	1447.28

accurate estimate of the separation distance by employing searching algorithms such as gradient method and golden section search method to locate the only local minimum.

Next, estimation processes with different $\hat{n}$ assumed in the algorithm are conducted at $z = 800$, 1000, and 1200 nm, in steps of 200 nm. The results are listed in Table I. It is found that when the assumption of the electrostatic force model is correct ($\hat{n} = n$), accurate separation distances can be obtained. As mentioned, although the absolute value of z is unknown, the step distance of the piezo movement can be measured. The differences in the estimated separation distances can only be correctly matched with the piezo movements when the correct model of the electrostatic force $\hat{n} = n = 1.2$ is assumed (Fig. 5). The mismatch is larger if there is a larger difference in the electrostatic force model. The differences in estimated separation distances are found to be 382.35 and 417.65 nm for $\hat{n} = 1.15$ and 1.25, respectively, when the piezo moves from $z = 800$ nm to $z = 1200$ nm. This means that if the measurement error of the piezo movement is less than 4%, then we will be able to determine the correct estimate of n with a resolution of $\delta n = 0.05$. In practice, the measurement error of the piezo can be greatly reduced by calibrations [44]. The voltage difference due to the electrostatic patch potential fluctuation is estimated to be $\hat{V}_1 = 10.0$ mV via Eq. (13), which is very accurate.

B. Noisy measurement data

Noise is always present in real measurements and any proposed calibration methods must be robust to noise. We also test the robustness of our method based on synthetic data. Gaussian noise with zero mean and standard deviation of 1 nm is added to $x(t)$. The noisy data $x(t)$ are then processed in our algorithm. The noisy $x(t)$ is plotted (Fig. 6) when the cantilever is vibrating at the equilibrium separation distance $z = 1200$ nm. It is found that the cost function $G(\hat{z})$ still has one local minimum. Our method has been tested with uncorrelated Gaussian noise sequences with zero mean and standard deviation of 1 nm. Statistically, the estimated separation distance is $\hat{z} = 1199.82 \pm 1.92$ nm. Estimations are also conducted when different electrostatic models are assumed at three equilibrium separation distances (Table II). Only one noise sequence is added to the trajectory $x(t)$ during the estimation processes. The differences in the estimated separation distances are plotted when the piezo moves from $z = 800$ nm to $z = 1200$ nm for different models of the electrostatic force assumed (Fig. 7). It could be seen that one is still able to identify the correct electrostatic force model by comparing the differences in the estimated separation distances with the piezo movements. The voltage difference due to electrostatic patch charge is calculated to be $\hat{V}_1 = 10.025$ mV at $z = 1200$ nm.

We point out that more accurate results could be obtained by filtering $x(t)$ properly to reduce the noise effect [45]. Alternatively, estimations could be carried out at different time intervals and estimates based on different intervals can be averaged. For uncorrelated noises, the average value of the estimates will have better accuracy and confidence level.

V. CONCLUSION

In this paper, an electrostatic calibration method for Casimir force measurements based on large-amplitude dynamic force measurement is introduced. The proposed electrostatic calibration method relies on signal processing algorithms to estimate the unknown system parameters such as the absolute separation distance and to identify the correct electrostatic force model when one of the interaction surfaces is vibrating at large amplitudes. There are several advantages when compared to the conventional method. First of all, the measurement sensitivity is greatly enhanced, as our proposed calibration is conducted at smaller separations where the electrostatic force is stronger. Second, as large-amplitude dynamic force measurements are performed, our method is much more robust to noise and drift. It is proven in theory and numerical studies that it is able to obtain an accurate estimate of the absolute separation distance and identify the correct electrostatic force model.

APPENDIX: PROOF OF EQUATIONS (9)–(11)

In this section, we will prove that the proposed cost function $G(\hat{z})$ has the properties described by Eqs. (9)–(11) under normal operation conditions if the positive functions $F_c(x)$ and $F_e(x)$ with $x > 0$ satisfy Eq. (12).

TABLE II. Estimated separation distance (nm) when the measurement is subject to noise.

z (nm)	$\hat{n}$ =0.9	$\hat{n}$ =1	$\hat{n}$ =1.1	$\hat{n}$ =1.2	$\hat{n}$ =1.3	$\hat{n}$ =1.4	$\hat{n}$ =1.5
800 (nm)	688.51	722.48	759.82	800.72	844.63	891.00	940.06
1000 (nm)	840.43	889.66	943.31	1001.43	1062.88	1127.73	1194.88
1200 (nm)	990.32	1055.60	1126.38	1202.15	1281.96	1364.89	1450.13

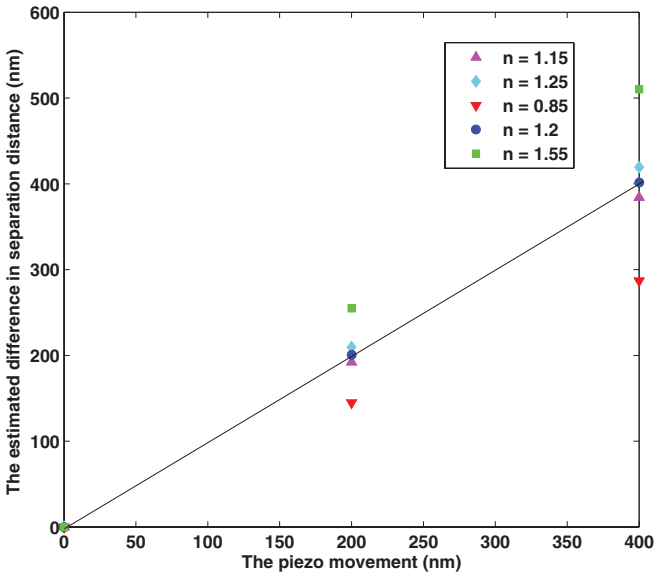

FIG. 7. (Color online) The estimated piezo movement with respect to different $\hat{n}$ when the separation distance is changed from 800 nm to 1200 nm and the measurement is subject to noise.

When $\gamma_1 > \sqrt{k/m}$, the second-order filters described by Eqs. (4)–(7) are overdamped, which leads to

$$y(t) = \int_0^t Q(t-\tau)\left[V_1^2 \frac{F_e(z+x(\tau))}{m} + \frac{F_c(z+x(\tau))}{m}\right] d\tau, \tag{A1}$$

$$\xi_1(t) = \int_0^t Q(t-\tau)\frac{F_e(\hat{z}+x(\tau))}{m} d\tau, \tag{A2}$$

$$\xi_2(t) = \int_0^t Q(t-\tau)\frac{F_c(\hat{z}+x(\tau))}{m} d\tau, \tag{A3}$$

where $Q(t-\tau) = (\frac{e^{-\alpha(t-\tau)} - e^{-\beta(t-\tau)}}{\beta-\alpha})$, $\alpha = \gamma_1 - \sqrt{\gamma_1^2 - \omega_0^2}$, and $\beta = \gamma_1 + \sqrt{\gamma_1^2 - \omega_0^2}$. Under normal operation condition, the trajectory $x(t)$ is dominated by the fundamental sinusoidal, which could be expressed as $x(t) = A\sin(\omega t + \phi) + d_0$. This leads to

$$\begin{aligned}\frac{F_c(z+x(t))}{m} &= \frac{F_c(z+d_0+A\sin(\omega t+\phi))}{m} \\ &= \frac{L_0(z)}{m} + \sum_{i=1}^{+\infty}\frac{L_i(z)}{m}\sin(i\omega t + \phi_i) \\ &\approx \frac{L_0(z)}{m} + \frac{L_1(z)}{m}\sin(\omega t+\phi),\end{aligned} \tag{A4}$$

where $L_0(z) = \frac{1}{T}\int_0^T F_c(z+d_0+A\sin(\omega t+\phi))dt$, $L_i(z) = \frac{1}{T}\int_0^T 2F_c(z+d_0+A\sin(\omega t+\phi))\sin(i\omega t+\phi_i)dt, \phi_i = \phi\,(i = 1,3,5,\ldots)$, and $\phi_i = \phi + \frac{\pi}{2}\,(i = 2,4,6,\ldots)$. Higher-order harmonics are neglected in our analysis as they are much smaller than the signal at fundament frequency. Similarly, we can denote

$$\frac{\partial\frac{F_c(z+x(t))}{m}}{\partial z} \approx \frac{l_0(z)}{m} + \frac{l_1(z)}{m}\sin(\omega t+\phi), \tag{A5}$$

$$\frac{F_e(z+x(t))}{m} \approx \frac{N_0(z)}{m} + \frac{N_1(z)}{m}\sin(\omega t+\phi), \tag{A6}$$

$$\frac{\partial\frac{F_e(z+x(t))}{m}}{\partial z} \approx \frac{n_0(z)}{m} + \frac{n_1(z)}{m}\sin(\omega t+\phi), \tag{A7}$$

where $l_0(z) = \frac{1}{T}\int_0^T \frac{\partial F_c(z+d_0+A\sin(\omega t+\phi))}{\partial z}dt$, $l_1(z) = \frac{1}{T}\int_0^T 2\frac{\partial F_c(z+d_0+A\sin(\omega t+\phi))}{\partial z}\sin(\omega t+\phi)dt$, $N_0(z) = \frac{1}{T}\int_0^T F_e(z+d_0+A\sin(\omega t+\phi))dt$, $N_1(z) = \frac{1}{T}\int_0^T 2F_e(z+d_0+A\sin(\omega t+\phi))\sin(\omega t+\phi)dt$, $n_0(z) = \frac{1}{T}\int_0^T \frac{\partial F_e(z+d_0+A\sin(\omega t+\phi))}{\partial z}dt$, and $n_1(z) = \frac{1}{T}\int_0^T 2\frac{\partial F_e(z+d_0+A\sin(\omega t+\phi))}{\partial z}\sin(\omega t+\phi)dt$. The steady state of the filter outputs can be calculated as

$$\begin{aligned}y(t) - \xi_2(t) = &\frac{L_0(z) - L_0(\hat{z}) + V_1^2 N_0(z)}{k} \\ &+ p\big[L_1(z) - L_1(\hat{z}) + V_1^2 N_1(z)\big]\sin(\omega t+\varphi),\end{aligned} \tag{A8}$$

$$-\frac{\partial\xi_2(t)}{\partial\hat{z}} = \frac{-l_0(\hat{z})}{k} + p[-l_1(\hat{z})]\sin(\omega t+\varphi), \tag{A9}$$

$$\xi_1(t) = \frac{N_0(\hat{z})}{k} + pN_1(\hat{z})\sin(\omega t+\varphi), \tag{A10}$$

$$\frac{\partial\xi_1(t)}{\partial\hat{z}} = \frac{n_0(\hat{z})}{k} + pn_1(\hat{z})\sin(\omega t+\varphi), \tag{A11}$$

where $p = \frac{1}{\sqrt{(m\omega^2-k)^2+(2\gamma_1 m\omega)^2}}$ and $\varphi = \phi - \tan^{-1}[2\gamma_1 m\omega/(k-m\omega^2)]$.

From the Cauchy-Schwartz inequality, we have

$$\begin{aligned}&\int_{t_1}^{t_2}[y(t)-\xi_2(t)]^2 dt \int_{t_1}^{t_2}\big[\xi_1^2(t)\big]dt \\ &\quad\geqslant \left(\int_{t_1}^{t_2}\{[y(t)-\xi_2(t)]\xi_1(t)\}dt\right)^2.\end{aligned} \tag{A12}$$

The equality is valid only when $\hat{z} = z$. Thus, we can conclude that the cost function $G(\hat{z})$ will be equal to zero only when $\hat{z} = z$ and will be positive otherwise. The first derivative of $G(\hat{z})$ with respect to $\hat{z}$ can be expressed as

$$\begin{aligned}\frac{dG(\hat{z})}{d\hat{z}} = &\frac{2}{\left\{\int_{t_1}^{t_2}\big[\xi_1^2(t)\big]dt\right\}^2}\left[\int_{t_1}^{t_2}\{[y(t)-\xi_2(t)]\xi_1(t)\}dt\left(\int_{t_1}^{t_2}\{[y(t)-\xi_2(t)]\xi_1(t)\}dt\int_{t_1}^{t_2}\left[\frac{\partial\xi_1(t)}{\partial\hat{z}}\xi_1(t)\right]dt\right.\right. \\ &-\int_{t_1}^{t_2}\left\{[y(t)-\xi_2(t)]\frac{\partial\xi_1(t)}{\partial\hat{z}}\right\}dt\int_{t_1}^{t_2}\big[\xi_1^2(t)\big]dt\Bigg) + \int_{t_1}^{t_2}\big[\xi_1^2(t)\big]dt\left\{\int_{t_1}^{t_2}[y(t)-\xi_2(t)]\left[-\frac{\partial\xi_2(t)}{\partial\hat{z}}\right]dt\int_{t_1}^{t_2}\big[\xi_1^2(t)\big]dt\right. \\ &\left.\left.-\int_{t_1}^{t_2}[y(t)-\xi_2(t)]\xi_1(t)dt\int_{t_1}^{t_2}[\xi_1(t)]\left[-\frac{\partial\xi_2(t)}{\partial\hat{z}}\right]dt\right\}\right].\end{aligned} \tag{A13}$$

It is easy to show that $\int_{t_1}^{t_2}\left[\xi_1^2(t)\right]dt > 0$. And it is mentioned in the paper that the estimate $\hat{z}$ is chosen to ensure that $\int_{t_1}^{t_2}[y(t) - \xi_2(t)]\xi_1(t)dt > 0$. The period $[t_1,t_2]$ is chosen to satisfy $t_2 - t_1 = NT$. It is easy to verify that

$$\int_{t_1}^{t_2}\{[y(t)-\xi_2(t)]\xi_1(t)\}dt\int_{t_1}^{t_2}\left[\frac{\partial\xi_1(t)}{\partial\hat{z}}\xi_1(t)\right]dt - \int_{t_1}^{t_2}\left\{[y(t)-\xi_2(t)]\frac{\partial\xi_1(t)}{\partial\hat{z}}\right\}dt\int_{t_1}^{t_2}\left[\xi_1^2(t)\right]dt$$
$$= \frac{NT^2p^2}{2k^2}\left\{\left[L_0(z)-L_0(\hat{z})+V_1^2N_0(z)\right]N_1(\hat{z}) - \left[L_1(z)-L_1(\hat{z})+V_1^2N_1(z)\right]N_0(\hat{z})\right\}[N_0(\hat{z})n_1(\hat{z}) - N_1(\hat{z})n_0(\hat{z})], \quad \text{(A14)}$$

and

$$\int_{t_1}^{t_2}[y(t)-\xi_2(t)]\left[-\frac{\partial\xi_2(t)}{\partial\hat{z}}\right]dt\int_{t_1}^{t_2}\left[\xi_1^2(t)\right]dt - \int_{t_1}^{t_2}[y(t)-\xi_2(t)\xi_1(t)]dt\int_{t_1}^{t_2}\xi_1(t)\left[-\frac{\partial\xi_2(t)}{\partial\hat{z}}\right]dt$$
$$= \frac{NT^2p^2}{2k^2}\left\{\left[L_0(z)-L_0(\hat{z})+V_1^2N_0(z)\right]N_1(\hat{z}) - \left[L_1(z)-L_1(\hat{z})+V_1^2N_1(z)\right]N_0(\hat{z})\right\}[N_0(\hat{z})l_1(\hat{z}) - N_1(\hat{z})l_0(\hat{z})]. \quad \text{(A15)}$$

Further examinations of Eqs. (A14) and (A15) are taken:

$$[N_0(\hat{z})n_1(\hat{z}) - N_1(\hat{z})n_0(\hat{z})]$$
$$= \frac{1}{T^2}\int_0^T\int_0^T\left\{\left[F_e(\hat{z}+d_0+A\sin(\omega\tau_1+\phi))\frac{\partial F_e(\hat{z}+d_0+A\sin(\omega\tau_2+\phi))}{\partial\hat{z}}\right.\right.$$
$$\left.\left. - F_e(\hat{z}+d_0+A\sin(\omega\tau_2+\phi))\frac{\partial F_e(\hat{z}+d_0+A\sin(\omega\tau_1+\phi))}{\partial\hat{z}}\right][\sin(\omega\tau_2+\phi)-\sin(\omega\tau_1+\phi)]\right\}d\tau_1d\tau_2, \quad \text{(A16)}$$

$$[N_0(\hat{z})l_1(\hat{z}) - N_1(\hat{z})l_0(\hat{z})]$$
$$= \frac{1}{T^2}\int_0^T\int_0^T\left\{\left[F_e(\hat{z}+d_0+A\sin(\omega\tau_1+\phi))\frac{\partial F_c(\hat{z}+d_0+A\sin(\omega\tau_2+\phi))}{\partial\hat{z}}\right.\right.$$
$$\left.\left. - F_e(\hat{z}+d_0+A\sin(\omega\tau_2+\phi))\frac{\partial F_c(\hat{z}+d_0+A\sin(\omega\tau_1+\phi))}{\partial\hat{z}}\right][\sin(\omega\tau_2+\phi)-\sin(\omega\tau_1+\phi)]\right\}d\tau_1d\tau_2, \quad \text{(A17)}$$

$$[N_0(z)N_1(\hat{z}) - N_1(z)N_0(\hat{z})]$$
$$= \frac{1}{T^2}\int_0^T\int_0^T\{[F_e(z+d_0+A\sin(\omega\tau_1+\phi))F_e(\hat{z}+d_0+A\sin(\omega\tau_2+\phi))$$
$$-F_e(z+d_0+A\sin(\omega\tau_2+\phi))F_e(\hat{z}+d_0+A\sin(\omega\tau_1+\phi))][\sin(\omega\tau_2+\phi)-\sin(\omega\tau_1+\phi)]\}d\tau_1d\tau_2, \quad \text{(A18)}$$

$$[L_0(z)-L_0(\hat{z})]N_1(\hat{z}) - [L_1(z)-L_1(\hat{z})]N_0(\hat{z})$$
$$= \frac{1}{T^2}\int_0^T\int_0^T(\{[F_c(z+d_0+A\sin(\omega\tau_1+\phi)) - F_c(\hat{z}+d_0+A\sin(\omega\tau_1+\phi))]$$
$$\times F_e(\hat{z}+d_0+A\sin(\omega\tau_2+\phi)) - [F_c(z+d_0+A\sin(\omega\tau_2+\phi)) - F_c(\hat{z}+d_0+A\sin(\omega\tau_2+\phi))]$$
$$\times F_e(\hat{z}+d_0+A\sin(\omega\tau_1+\phi))\}[\sin(\omega\tau_2+\phi)-\sin(\omega\tau_1+\phi)])d\tau_1d\tau_2. \quad \text{(A19)}$$

Next, we will prove the following theorem:

Theorem 1. If the positive functions $F_c(x)$ and $F_e(x)$ with $x > 0$ satisfy the following conditions:

$$\frac{d\frac{dF_e(x)/dx}{F_e(x)}}{dx} > 0, \quad \text{(A20)}$$

$$\frac{d\frac{dF_e(x)/dx}{F_e(x)}}{dx} > 0, \quad \text{(A21)}$$

$$\frac{d\frac{dF_c(x)/dx}{F_c(x)}}{dx} > 0, \quad \text{(A22)}$$

$$\frac{d\frac{F_c(x)}{F_e(x)}}{dx} < 0, \quad \text{(A23)}$$

$$\frac{dF_c(x)}{dx} < 0, \quad \text{(A24)}$$

then Eqs. (9)–(11) are valid.

Proof. It is easy to verify that Eq. (A20) is equivalent to the following equation:

$$\frac{\frac{dF_e(x+\Delta)}{dx}}{F_e(x+\Delta)} - \frac{\frac{dF_e(x)}{dx}}{F_e(x)} > 0, \quad \text{(A25)}$$

where $\Delta > 0$ is a constant. This is equivalent to

$$\frac{dF_e(x+\Delta)}{dx}F_e(x) - \frac{dF_e(x)}{dx}F_e(x+\Delta) > 0. \quad \text{(A26)}$$

Similarly, we can obtain the following equation:

$$\frac{dF_e(x-\Delta)}{dx}F_e(x) - \frac{dF_e(x)}{dx}F_e(x-\Delta) < 0. \quad \text{(A27)}$$

By substituting $x = \hat{z}+d_0+A\sin(\omega\tau_1+\phi), \Delta = |A\sin(\omega\tau_2+\phi) - A\sin(\omega\tau_1+\phi)|$ into the two equations above, we can prove that

$$[N_0(\hat{z})n_1(\hat{z}) - N_1(\hat{z})n_0(\hat{z})] > 0. \quad \text{(A28)}$$

Further transformation of Eq. (A25) leads to

$$\frac{d[F_e(x+\Delta)/F_e(x)]}{dx} > 0, \tag{A29}$$

which is equivalent to

$$F_e(x_1+\Delta)F_e(x_2) - F_e(x_2+\Delta)F_e(x_1) > 0 (x_1 > x_2). \tag{A30}$$

In the same way, we can obtain the following equation:

$$F_e(x_1-\Delta)F_e(x_2) - F_e(x_2-\Delta)F_e(x_1) < 0 (x_1 > x_2). \tag{A31}$$

By substituting $x_1 = \hat{z} + d_0 + A\sin(\omega\tau_1 + \phi)$, $x_2 = \hat{z} + d_0 + A\sin(\omega\tau_2 + \phi)$, and $\Delta = |\hat{z} - z|$ into Eq. (A18), we can show that

$$[N_0(z)N_1(\hat{z}) - N_1(z)N_0(\hat{z})][\hat{z} - z] > 0. \tag{A32}$$

Similarly, we can show that Eq. (A21) can lead to

$$[N_0(\hat{z})l_1(\hat{z}) - N_1(\hat{z})l_0(\hat{z})] > 0. \tag{A33}$$

Based on Eq. (A22), we get

$$\left[\frac{dF_c(x+\Delta)}{dx}F_c(x) - \frac{dF_c(x)}{dx}F_c(x+\Delta)\right] \Big/ F_c^2(x+\Delta) > 0. \tag{A34}$$

Together with Eqs. (A23) and (A24), we can obtain

$$\frac{d\left[\frac{F_c(x)-F_c(x+\Delta)}{F_c(x+\Delta)}\frac{F_c(x+\Delta)}{F_e(x+\Delta)}\right]}{dx} < 0. \tag{A35}$$

This is equivalent to

$$\frac{d\left[\frac{F_c(x)-F_c(x+\Delta)}{F_e(x+\Delta)}\right]}{dx} < 0. \tag{A36}$$

Similarly, we can obtain

$$\frac{d\left[\frac{F_c(x)-F_c(x-\Delta)}{F_e(x-\Delta)}\right]}{dx} > 0. \tag{A37}$$

Based on Eqs. (A36) and (A37), we can prove that

$$\{[L_0(z) - L_0(\hat{z})]N_1(\hat{z}) - [L_1(z) - L_1(\hat{z})]N_0(\hat{z})\}[\hat{z} - z] > 0. \tag{A38}$$

With Eqs. (A28), (A32), (A33), and (A38), it can be shown directly that Eqs. (9)–(11) are valid.

[1] H. B. G. Casimir, Proc. K. Ned. Akad. Wet. **51**, 793 (1948).
[2] F. Chen, U. Mohideen, G. L. Klimchitskaya, and V. M. Mostepanenko, Phys. Rev. A **66**, 032113 (2002).
[3] B. Geyer, G. L. Klimchitskaya, and V. M. Mostepanenko, Phys. Rev. A **65**, 062109 (2002).
[4] A. W. Rodriguez, F. Capasso, and S. G. Johnson, Nature Photon. **5**, 211 (2011).
[5] R. S. Decca, D. Lopez, H. B. Chan, E. Fischbach, D. E. Krause, and C. R. Jamell, Phys. Rev. Lett. **94**, 240401 (2005).
[6] G. L. Klimchitskaya and V. M. Mostepanenko, Contemp. Phys. **47**, 131 (2006).
[7] R. W. Johnstone and M. Parameswaran, J. Micromech. Microeng. **12**, 855 (2002).
[8] U. Mohideen and A. Roy, Phys. Rev. Lett. **81**, 4549 (1998).
[9] H. B. Chan *et al.*, Science **291**, 1941 (2001).
[10] S. K. Lamoreaux, Phys. Rev. Lett. **78**, 5 (1997).
[11] M. J. Sparnaay, Physica **24**, 751 (1958).
[12] M. Brown-Hayes, D. A. R. Dalvit, F. D. Mazzitelli, W. J. Kim, and R. Onofrio, Phys. Rev. A **72**, 052102 (2005).
[13] A. Roy and U. Mohideen, Phys. Rev. Lett. **82**, 4380 (1999).
[14] H. B. Chan, Y. Bao, J. Zou, R. A. Cirelli, F. Klemens, W. M. Mansfield, and C. S. Pai, Phys. Rev. Lett. **101**, 030401 (2008).
[15] S. de Man, K. Heeck, R. J. Wijngaarden, and D. Iannuzzi, Phys. Rev. Lett. **103**, 040402 (2009).
[16] C. Hertlein, L. Helden, A. Gambassi, S. Dietrich, and C. Bechinger, Nature (London) **451**, 172 (2007).
[17] A. O. Sushkov, W. J. Kim, D. A. R. Dalvit, and S. K. Lamoreaux, Nature Phys. **7**, 230 (2011).
[18] I. E. Dzyaloshinskii, E. M. Lifshitz, and L. P. Pitaevskii, Adv. Phys. **10**, 165 (1961).
[19] O. Kenneth, I. Klich, A. Mann, and M. Revzen, Phys. Rev. Lett. **89**, 033001 (2002).
[20] U. Leonhardt and T. G. Philbin, New J. Phys. **9**, 254 (2007).
[21] J. N. Munday, F. Capasso, and V. A. Parsegian, Nature (London) **457**, 170 (2009).
[22] V. Yannopapas and N. V. Vitanov, Phys. Rev. Lett. **103**, 120401 (2009).
[23] A. G. Grushin and A. Cortijo, Phys. Rev. Lett. **106**, 020403 (2011).
[24] S. K. Lamoreaux, Lect. Notes Phys. **834**, 219 (2011).
[25] G. L. Klimchitskaya, M. Bordag, E. Fischbach, D. E. Krause, and V. M. Mostepanenko, Int. J. Mod. Phys. A **26**, 3918 (2011).
[26] D. Iannuzzi, M. Lisanti, J. N. Munday, and F. Capasso, Solid State Commun. **135**, 618 (2005).
[27] H.-C. Chiu, C.-C. Chang, R. Castillo-Garza, F. Chen, and U. Mohideen, J. Phys. A **41**, 164022 (2008).
[28] R. S. Decca, E. Fischbach, G. L. Klimchitskaya, D. E. Krause, D. Lópes, U. Mohideen, and V. M. Mostepanenko, Int. J. Mod. Phys. A **26**, 3930 (2011).
[29] W. J. Kim, M. Brown-Hayes, D. A. R. Dalvit, J. H. Brownell, and R. Onofrio, Phys. Rev. A **78**, 020101 (2008).
[30] W. J. Kim, A. O. Sushkov, D. A. R. Dalvit, and S. K. Lamoreaux, Phys. Rev. A **81**, 022505 (2010).
[31] R. Garcia and R. Perez, Surf. Sci. Rep. **47**, 191 (2002).
[32] S. de Man, K. Heeck, and D. Iannuzzi, Phys. Rev. A **79**, 024102 (2009).
[33] H. B. Chan, V. A. Aksyuk, R. N. Kleiman, D. J. Bishop, and F. Capasso, Phys. Rev. Lett. **87**, 211801 (2001).
[34] M. Serry, D. Alliser, and J. Maclay, J. Microelectromech. Syst. **4**, 193 (1995).

[35] S. Cui and Y. C. Soh, J. Microelectromech. Syst. **19**, 1153 (2010).
[36] S. Cui and Y. C. Soh, Phys. Lett. A **376**, 109 (2011).
[37] R. O. Behunin, F. Intravaia, D. A. R. Dalvit, P. A. Maia Neto, and S. Reynaud, Phys. Rev. A **85**, 012504 (2012).
[38] A. Lambrecht and S. Reynaud, Eur. Phys. J. D **8**, 309 (2000).
[39] S. Cui and Y. C. Soh, Phys. Rev. A **82**, 062510 (2010).
[40] V. B. Bezerra, G. L. Klimchitskaya, and V. M. Mostepanenko, Phys. Rev. A **62**, 014102 (2000).
[41] M. L. Heath, *Scientific Computing: An Introductory Survey* (McGraw-Hill, New York, 1997).
[42] C. C. Speake and C. Trenkel, Phys. Rev. Lett. **90**, 160403 (2003).
[43] S. K. Lamoreaux, arXiv:0808.0885v2.
[44] B. W. Harris, F. Chen, and U. Mohideen, Phys. Rev. A **62**, 052109 (2000).
[45] J. Legleiter, M. Park, B. Cusick, and T. Kowalewski, Proc. Natl. Acad. Sci. USA **103**, 4813 (2006).